

DPRed: Making Typical Activation Values Matter In Deep Learning Computing

Alberto Delmas Lascorz, Sayeh Sharify, Patrick Judd,
Milos Nikolic, Andreas Moshovos
Electrical and Computer Engineering, University of Toronto
{delmasl1, juddpatr, sayeh, moshovos}@ece.utoronto.ca,
milos.nikolic@mail.utoronto.ca

ABSTRACT

We show that selecting a fixed precision for *all* activations in Convolutional Neural Networks, even if that precision is different per layer, amounts to *worst case* design. We show that much lower precisions can be used, if we could target the *common case* instead by tailoring the precision at a much finer granularity than that of a layer. We propose *Dynamic Prediction Reduction (DPRed)* where hardware on-the-fly detects the precision activations need and at a much finer granularity than a whole layer. We demonstrate a practical implementation of *DPRed* with *DPRed Stripes (DPRS)* a data-parallel hardware accelerator that adjusts precision on-the-fly to accommodate the values of the activations it processes concurrently. *DPRS* accelerates convolutional layers and executes unmodified convolutional neural networks. *DPRS* is $2.61\times$ faster and $1.84\times$ more energy efficient than a fixed-precision accelerator for a set of convolutional neural networks. We further extend *DPRS* to exploit activation and weight precisions for fully-connected layers. The enhanced design improves average performance and energy efficiency respectively by $2.59\times$ and $1.19\times$ over the fixed-precision accelerator for a *broader* set of neural networks. We also consider a lower cost variant that supports only even precision widths which offers better energy efficiency.

This paper combines the previously proposed Dynamic Stripes [1] and Tartan [2] and includes a more detailed analysis of the precisions required at various granularities.

1. INTRODUCTION

Until very recently machines that can perform tasks that we typically associate with intelligence such as driving, identifying what images depict, or translating between languages seemed the stuff of science-fiction. Practical applications were of limited success. Yet, recently, Deep Learning [3] (DL) has been disrupting the boundary between fiction and reality. While advances in DL algorithms and the availability of massive amounts of data to train on are two of the key reasons that led to these successes, computing hardware perfor-

mance is the third. It is only very recently that the computing performance of general-purpose graphics processing units has reached a level that enabled a leap on what was practical with DL [4]. Given the disruptive potential of DL sustaining further advances in hardware performance and energy efficiency for DL workloads has justifiably attracted significant attention. As Dennard scaling has ceased [5], hardware acceleration for DL has emerged as a viable approach for further enabling DL innovation.

Early successes in hardware acceleration for DL relied on exploiting its computation structure, e.g., [6, 7, 8]. Many recent DL hardware accelerators exploit the various forms of *informational inefficiency* that deep learning neural networks (DNNs) exhibit. It has been found that informational inefficiency manifests in DNNs as ineffectual neurons [9, 10], activations [9, 11, 10], or weights [12, 10], as an excess of precision, e.g., [13, 14, 15, 16, 17, 18], as ineffectual activation bits [19], or in general as over-provisioning, e.g., [20]. Whether these inefficiencies are best exploited statically, dynamically, or both is an open question. Furthermore, which forms of inefficiency will persist as DNNs evolve remains to be seen.

These past successes demonstrate that at this stage of our exploration on how to best deliver the hardware performance advances needed to support DL innovation, identifying DNN properties that hardware and/or software could potentially exploit is invaluable. Accordingly, the key contribution of this work is that it highlights an overlooked property of the activation stream of DNNs. Further, to prove that this property can enable practical applications, we present one.

Specifically, this work shows that the precision needed by activations varies considerably at runtime and much more than what can be discerned through profiling. It has been known that DNNs exhibit variable precision requirements across networks and within networks at the layer level. This per layer variability has been exploited at the hardware level in several ways. Some designs hardwire the precision [13] per layer, others scale voltage and frequency per layer [21], or support several data widths [22], or even support the full spectrum of bit-widths [18]. All aforementioned designs 1) exploit precision at the granularity of a layer and 2) use precisions that are derived through profiling. As a result,

This paper was originally submitted to HPCA-24 in August 2017 and subsequently revised to include the motivation section. It was also submitted to ISCA-18 in November 2017. A revised version is under review at another conference.

profile-based analysis results in precisions that must accommodate *any possible input* and for *any* activation across a *whole* layer. We observe that this corresponds to a *worst case* precision analysis that exacerbates the importance of the larger, yet infrequent activation values. We show that much higher potential for improvement exists if we tailor precision to target the *common case* instead.

We observe that the precision used at any given point of time needs to accommodate: 1) the activation values for the *specific* input at hand, and further 2) only the activation values that are being processed concurrently. As a result the precision used can vary with the input and could be adapted at a much finer granularity than the layer. We demonstrate that indeed, depending on how many activations are grouped together during processing, the precision that they need can be much lower than that identified through profiling. Accordingly, an accelerator that incorporates *Dynamic Precision Reduction* or *DPRed* (pronounced “Deep Red”) can further boost performance and energy efficiency over one that merely uses profile-derived per layer precisions.

To demonstrate that the aforementioned activation value property can be of practical use we present *DPRed Stripes* (*DPRS*), an accelerator whose performance varies proportionally with precision at the granularity of a processing group. For this purpose we build upon the *Stripes* accelerator [18] which exploits per-layer profile-derived precisions. While the hardware changes needed by *DPRS* prove modest the resulting performance and energy efficiency improvements are anything but. For example, compared to a fixed-precision accelerator *DPNN* (see Section 3.1) and for a configuration that performs $4K\ 16b \times 16b$ multiplications per cycle, *STR* improves average performance and energy efficiency by $1.9\times$ and $1.32\times$ respectively while *DPRS* improves performance by $2.6\times$ and $1.84\times$. For configurations using a smaller processing group size the performance improvements can be as high as $2.84\times$.

As with *Stripes*, *DPRS* benefits convolutional layers (CVLs) only. While CVLs dominate execution time in many image related applications such as for example in classification using convolutional neural networks (CNNs) [7], fully-connected layers (FCLs) are more prevalent in other DNN applications. For example, two networks that represent 61% of Google’s TPU datacenter usage employ FCLs exclusively [22]. As an additional contribution we also show how precision variability can be used to accelerate FCLs. Specifically, we present *TARTAN* (*TRT*) which enables *DPRS* to exploit precision excess also for FCLs. In an FCL *TRT* is $P/\max(P_w, P_a)$ faster than *STR* and *DPNN* where P is the maximum precision supported in hardware, and P_a and P_w are the precisions for the weights and the activations respectively. While we study *TRT* in conjunction with *DPRed* the two techniques can be used independently. However, *TRT* will benefit from *DPRed* when $P_a > P_w$ for a set of concurrently processed activations and weights. Experiments show that when combined with *DPRS*, *TRT* improves performance over *DPNN* by $2.59\times$ and $1.19\times$ over the fixed-precision accelerator for a *broad*er set of neural networks.

In a 65nm technology, *DPRS* requires less than 1% more area than *STR*, while adding *TRT* requires 51% more area. In either case, improvements with *DPRS* alone, or with *DPRS*

combined with *TRT* far exceed those possible by scaling *DPNN* to use the same area.

In summary, this work makes the following contributions: 1) It characterizes the precision needed by several CNNs at various granularities that are much smaller than a layer. It demonstrates that on average the precision needed is much narrower than the per layer profile derived precision used in past work. 2) It demonstrates a practical application of the aforementioned property with *DPRS*. 3) It demonstrates how to exploit precision variability for FCLs with *TRT*.

The rest of this paper is organized as follows: Sections 2 analyzes the runtime precision needs of activations in CNNs. Section 3 presents *DPRS* while Section 4 presents *TRT*. Section 5 reports the performance, energy efficiency and area of our designs. Section 6 comments on related work while Section 7 concludes.

2. DYNAMIC PRECISION VARIABILITY

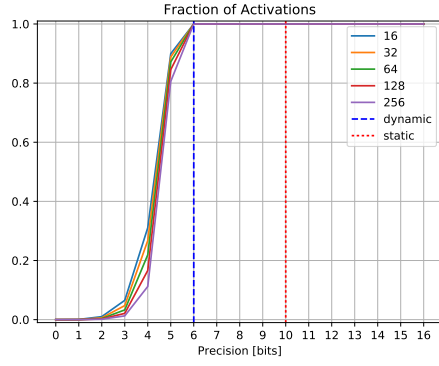
This section demonstrates that using per layer precisions for the activations is overly pessimistic. Much lower precisions are needed if we take into account the specific input and we narrow attention to a few activations at a time.

Figures 1a-1f show precision measurements for six CVLs two from each of AlexNet, GoogleNet, and SkimCaffe-ResNet50 [23]. The latter is a weight pruned network. We highlight these six layers for clarity since similar trends were observed in other networks and layers. The measurements are averaged over 50 different input images (except for the “dynamic” precision – see below). The graphs show the cumulative distribution of the precisions needed per group of activations for various group sizes ranging from 16 to 256. Two vertical lines report the precisions possible when considering all activation values for the whole layer: 1) the profile-derived (“static”), and 2) the one that can be detected dynamically (“dynamic”) for one image (we include this measurement to show that the precision can vary significantly also depending on the specific input).

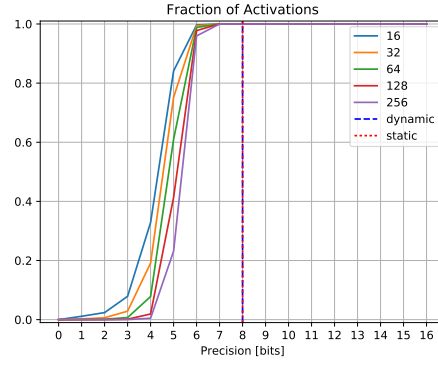
Figure 1a reports measurements for conv1, the first CVL of AlexNet. The statically profile-determined precision is 9 bits while all values within the layer could be represented with just 6 bits, an improvement of 33% in precision length. The cumulative distribution of the precisions needed per group of 256 activations shows that further reduction in precision is possible. For example, about 80% of these groups require 5 bits only, and about 15% just 4 bits. Smaller group sizes further reduce the *effective* precision, however, the differences are modest. These results suggest that indeed picking a precision for the whole layer exacerbates the importance of a few high-magnitude activations.

Figure 1b shows that for conv5 of AlexNet the profile-derived precision for the whole layer whether detected dynamically or derived statically is on average 8 bits. However, determining precision at even the 256 activation granularity yields a shorter effective precision for the layer. For example at least 95% of the activations can use just 5 bits a reduction of 37.5% in precision length. This result highlights that detecting precisions at a lower granularity than the layer is essential for some layers.

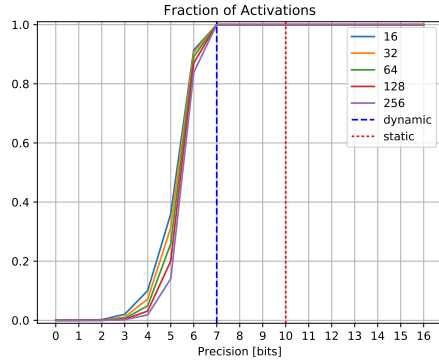
Conv1 of GoogLeNet in Figure 1c exhibits similar behavior to Conv1 of AlexNet. Layer 5a-1x1 in Figure 1d shows



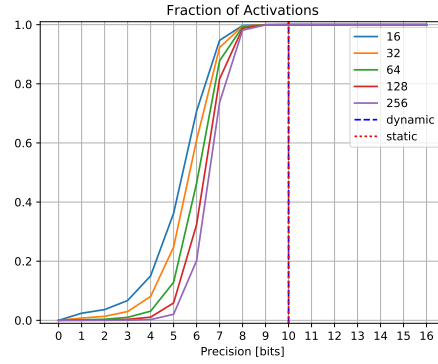
(a) AlexNet, Conv 1



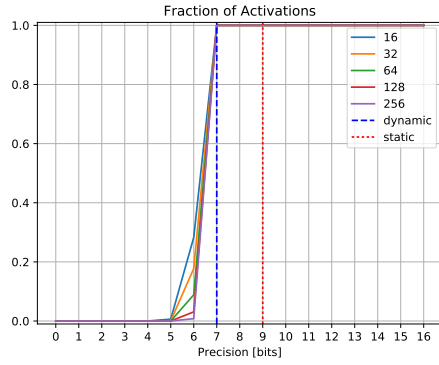
(b) AlexNet Conv 5



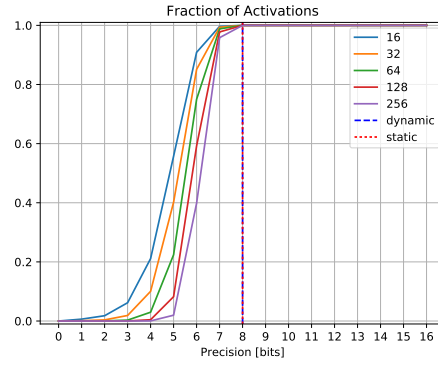
(c) GoogLeNet, Conv 1



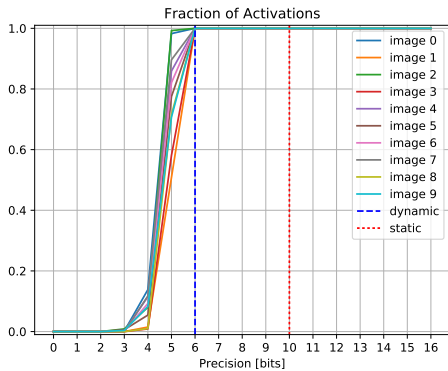
(d) GoogLeNet, 5a-1x1



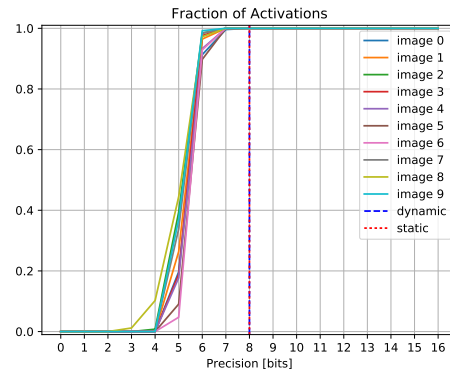
(e) SkimCaffe ResNet50, res3a_branch1



(f) SkimCaffe ResNet50, res5a_branch1



(g) AlexNet, Conv 1



(h) AlexNet Conv 5

Figure 1: Precision profiles for CVL layers from AlexNet, GoogLeNet, and Sparse ResNet50. (a)-(f) Average over multiple images. Multiple group sizes shown. (g)-(h): Per image variability with a group of 256 for AlexNet.

more pronounced improvements in effective precision with the smaller group sizes.

Figures 1e and 1f show that the behavior persists even in sparse networks where pruning has been used to eliminate most weights. We include this measurement to demonstrate that dynamic precision variability is a phenomenon that is orthogonal to weight sparsity and thus of potential value to designs that target sparse neural networks.

Figures 1g and 1h report the distribution of the precisions needed separately for 10 sample images. We restrict attention to the 256 activation group size for clarity. The measurements show that precision does indeed vary also with the input and considerably so. For Conv5 none of activations need more than 6 bits ever for these images whereas in Figure 1b some of the images from the larger sample included activation groups that needed 7 bits. These results highlight the second weakness of profile-derived per layer activations: they have to accommodate any possible input whereas in many practical applications there will be only some activations from only one input that will be processed concurrently.

Generally, for all the networks studied the following were observed: 1) The activation precision needed varies more so at the first layer, 2) for all layers the precisions needed at finer than a layer granularity are shorter than those needed for the whole layer, and 3) only a small number of activation groups require the maximum precision needed for the layer as a whole. These results motivate incorporating *dynamic prediction reduction* in hardware accelerators. In the rest of this work we focus on dense networks only. Combining the techniques we present with accelerators that exploit weight sparsity is interesting future work. Finally, while we studied convolutional neural networks only, it is likely that dynamic precision reduction would be useful also for other neural network architectures due to the expected activation value distributions. However, this has to be validated experimentally, a task that is left for future work.

3. DPRed STRIPES

We present a practical application where the fine-grain precision requirement variability of the activations is used to boost performance and energy efficiency. Specifically, this section presents *DPRS* an accelerator whose performance in CVLs scales proportionally with the inverse of the precision used in bits for activations. *DPRS* is unique in that it adjusts the precision on-the-fly to meet the needs of only those activations that are currently being processed. Fortunately, *DPRS* can be implemented as a modest extension over the previously proposed *Stripes* (*STR*) [18]. Accordingly, we first review *STR* and an equivalent fixed-precision accelerator, and then explain the changes needed to enable dynamic prediction reduction.

3.1 STRIPES and Bit-Parallel Accelerator

For clarity this discussion assumes the previously described configuration of an *STR* chip with 16 tiles, each processing 16 filters and 16 weights per filter and where the maximum precision for activations and weights is 16 bits (additional configurations are reported in the evaluation section). Figure 2a shows the tile of an equivalent

fixed-precision bit-parallel accelerator DPNN. DPNN and the memory system used for all designs are based on Da-DianNao [6]. In all designs, a *Dispatcher* fetches the activations from a central 4MB Activation Memory (AM) whereas a 2MB per tile slice of a Weight Memory (WM) provides the 4K weight bits that are needed per tile. Google’s TPU also uses large on-chip memories to avoid off-chip communication as much as possible [22]. In DPNN, the dispatcher broadcasts 16 activations, or 256 bits per cycle. Each cycle, each DPNN tile multiplies these 16 activations with 16 groups, each of 16 weights and accumulates the results into 16 output activations. Each group of weights corresponds to a different filter and there is one weight per input activation in each group. Each DPNN tile contains 16 inner-product units ($IP_{0...15}$) as shown.

In *STR*, each cycle the dispatcher broadcasts 16 sets of 16 activations to all tiles *bit-serially* for a total of 256 bits per cycle. Each activation set corresponds to a different input window so that the same 16 weights can be reused across groups to yield 16 output activations. As Figure 2b shows, each tile contains a grid of 16×16 Serial Inner-Product units (SIPs). Each SIP performs $16\text{ }1b \times 16b$ multiplications followed by a reduction. The SIPs along the same column share the same group of 16 single-bit activations, while the SIPs along the same row share the same 16 16b weights, as each SIP produces an output activation corresponding to a different window. Figure 2c shows one such row of SIPs. Overall, each tile accepts 256 input activation and $256 \times 16 = 4K$ weight bits per cycle, maintaining the same number of external wire connections as DPNN.

Before processing a layer *STR* expects software to specify the required precision, that is the positions of the most significant and of the least significant bits (MSB and LSB respectively), n^H and n^L . *STR* uses this precision for all activations within the layer. Since *STR* processes 256 activations bit-serially over P_a cycles, it can ideally improve performance by $16/P_a$ over the equivalent DPNN configuration that processes 16 16b activations per cycle.

3.2 DPRed Stripes Architecture

This section describes the modest changes needed over *STR* to implement dynamic precision reduction at the granularity of the 256 activations that are being processed concurrently. These are: 1) introducing a mechanism for detecting the precision needed per activation group, 2) adding a method of communicating the precision to the tiles, and 3) modifying the SIPs to appropriately handle starting the calculation *per group* at any n^H bit position.

Precision Detection: Figure 2d shows the *DPRS* organization. A *dispatcher* reads a group of 256 activations from AM, however before communicating their values bit-serially, it first inspects them detecting the precision needed. It then communicates this precision as a 4-bit offset and as a single *end of group* signal.

Figure 3 shows how the dispatcher adjusts n^H at runtime for an example group of four 16b activations A_0 through A_3 . The specific example activations can all be represented using just 12 bits as the highest bit position a 1 appears in any of them is at position 11. The precision detection unit calculates 16 signals, one per bit position, each being the OR of

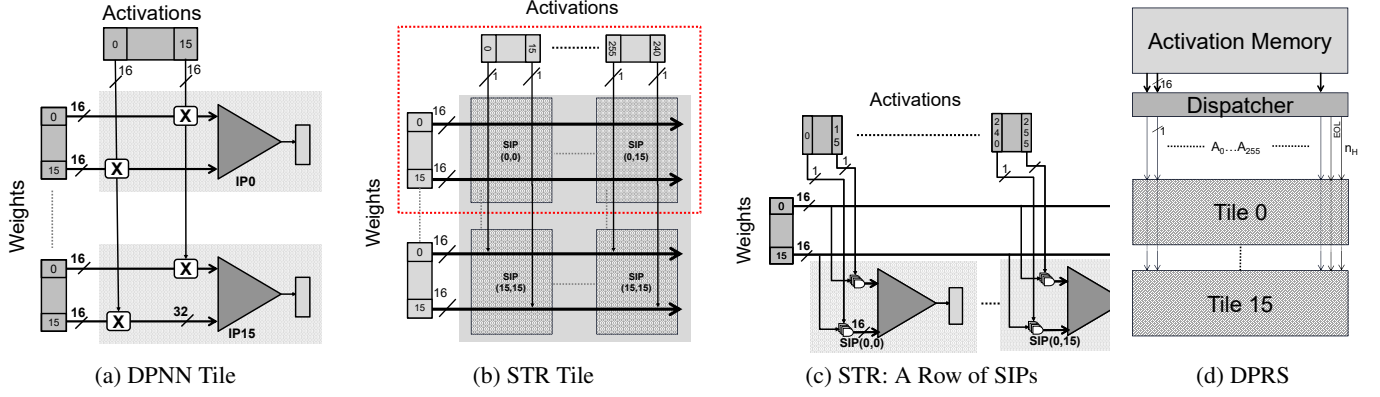


Figure 2: (a) Baseline bit-parallel accelerator. (b)-(d): DPRS: Converting *STR* to dynamically reduce activation precisions.

the corresponding bit values across all four activations. The implementation uses OR trees to generate these signals. A “leading 1” detector identifies the most significant bit that has a 1, and reports its position in 4 bits. The same method can detect n_L where a “trailing 1” encoder detects the least significant bit where a 1 appears. In practice, for the networks studied adjusting n_L dynamically resulted in negligible effective precision reduction of below 0.38% in all cases. This is expected as profiling can appropriately filter the less significant noisy bits which affect all activations regardless of their magnitude. Accordingly, the designs studied here use the profile-derived n_L per layer. The unit can be adapted to detect precisions for signed activations. This is useful with activation functions that do not clamp negative values.

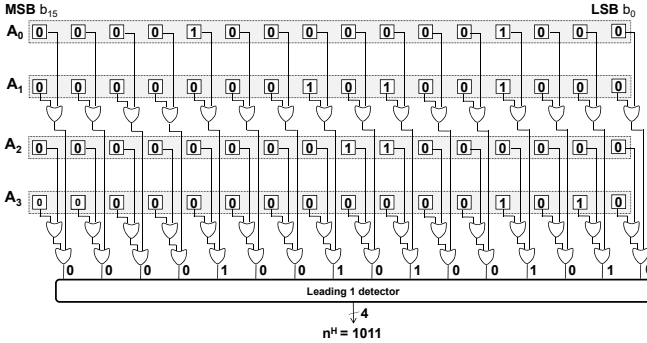


Figure 3: Dynamic Precision Reduction Unit Example.

Communicating the Precision: To process a group of activations, the dispatcher will send n_H as the starting offset for the activation group. The tiles will decrement this offset every subsequent cycle. The dispatcher will signal, using an *end of group* wire, the last cycle of processing for this group when the current offset becomes equal to n_L . Assuming that processing starts at the n_H bit, position, a counter keeps track of the current bit position being broadcast and a comparator sets the end of group signal when the counter arrives at n_L .

Granularity: In the example all concurrently processed activations are treated as one group. Equivalently, the *DPRS*

configurations studied in the rest of this work detect precision for all concurrently processed activations as a group. However, other arrangements are possible. For example, precision can be detected per group of 16 activations corresponding to SIPs along the same column. In such a case, once a group of activations is processed the corresponding SIPs can be made to wait for all other SIPs to finish before advancing to the next group of activations.

Modified Serial Inner-Product Unit: Figure 4 shows the modified SIP unit where an additional shifter appears at the adder tree output. This shifter, through the control signal s_B , adjusts the adder tree output so that it can be accumulated with the running sum in accumulator A aligning it at the appropriate bit position. This is necessary since starting position varies per activation group.

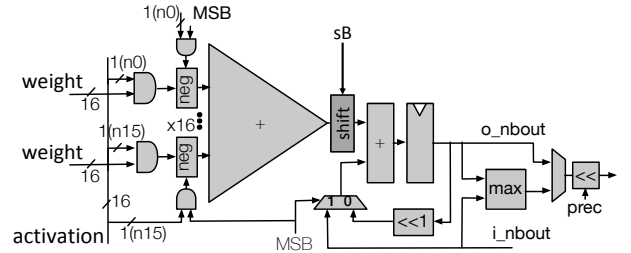


Figure 4: DPRS SIP.

4. FULLY-CONNECTED LAYERS

While *STR* and *DPRS* exploit precision variability for CVLs they do not do so for FCLs. As a result, performance for FCLs with *STR* and *DPRS* remains practically the same as that of DPNN, but energy-efficiency suffers. This section motivates further extending *STR* and for that *DPRS* to exploit precision variability to boost performance and energy efficiency for FCLs. We motivate this change by showing that: 1) indeed energy efficiency suffers in FCLs, (Section 4.1), and 2) precisions vary for weights in FCLs (Section 4.2). The aforementioned results motivate the *Tartan (TRT)* extension that improves performance and energy efficiency for

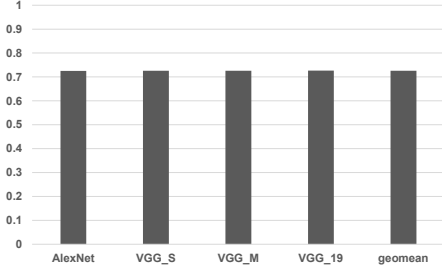


Figure 5: Energy Efficiency of *Stripes* compared to DPNN on Fully-Connected Layers.

FCLs and that complements *STR* and *DPRS*. For clarity this section presents *TRT* as an extension over *STR*.

4.1 Energy Efficiency in FCLs with STR

Figure 5 reports the energy efficiency of *STR* over that of DPNN for FCLs. Section 5.1 details the experimental methodology. While performance is virtually identical to DPNN, energy efficiency is on average $0.73\times$ compared to DPNN. While in image classification FCLs represent less than 10% of the overall execution time, in other workloads this is not the case. Accordingly, it is desirable to improve energy efficiency for these layers as well.

4.2 Precision Requirements

The per layer precision profiles presented here were found via the methodology of Judd *et al.* [14]. For the image classification convolutional neural networks, Caffe [24] was used to measure how reducing the precision of each FCL affects the network’s overall *top-1* prediction accuracy over 5000 images. The networks are taken from the Caffe Model Zoo [25] and are used as-is without retraining. For FCLs precision exploration was limited to cases where both P_w and P_a are equal (the weight and activation precision ranges differ). For CVLs only the activation precision is adjusted since none of the designs we consider can further boost performance when reducing the weight precisions. While reducing the weight precision for CVLs can reduce their memory footprint [26], we do not explore this option further in this work. For NeuralTalk, we measure BLEU scores when compared with the ground truth. For Denoise, we measure PSNR, and define 99% accuracy as a drop of no more than 0.04dB.

Table 1 reports the resulting per layer precisions separately for FCLs and CVLs. The ideal speedup columns report the performance improvement that would be possible if execution time could be reduced proportionally with precision compared to a 16-bit bit-parallel baseline. For the FCLs, the precisions required range from 8 to 10 bits and the potential for performance improvement is $1.64\times$ on average. If a 1% relative reduction in accuracy is acceptable then the performance improvement potential increases to $1.75\times$ on average. Given that the precision variability for FCLs is relatively low (ranges from 8 to 11 bits) one may be tempted to conclude that an 11-bit DPNN variant may be an appropriate compromise. However, given that the precision variability is

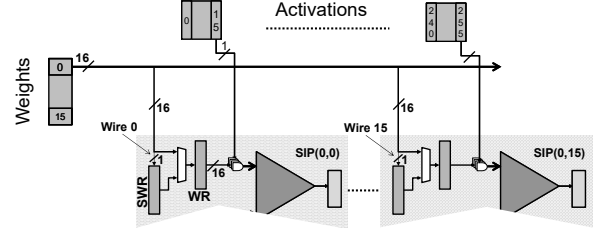


Figure 6: A row of a TRT tile.

much larger for the CVLs (range is 5 to 13 bits) the performance with a fixed precision datapath would be far below the ideal. Section 5 shows that the incremental cost of *TRT* over *STR* is well justified given the benefits.

4.3 TARTAN

Unfortunately, since there is no weight reuse in FCLs *STR* and for that *DPRS* cannot reuse the same weight over multiple windows to boost performance. In *DPRS* as in *STR* performance in FCLs is limited by the number of cycles needed to load a different set of weights per SIP column [18]. *TRT* overcomes this limitation and boosts performance even for FCLs by exploiting weight and activation precisions.

We use Figure 6 to explain the concept behind *TRT*’s operation. The figure shows a row of SIPs (similar to Figure 2c) and focuses on the first weight input only. Whereas in *STR* the 16b weight input to the AND gates was coming directly from the WM connection here it is connected to a 16b *Weight Register* (WR). A multiplexer selects from where the WR can load its contents. The first option is to do so directly from the WM wires as in *STR*. This maintains the functionality needed for CVLs. An extra pipeline stage is needed to accommodate loading first to WR (stage 1) and then “multiplying” with the activation (stage 2). The second option is to load WR from the 16b *Serial Weight Register* (SWR). The SWR has a single input wire connection to the WM signals which is different per SIP. The first SIP in the row connects to wire 0 while the last to wire 15. SWR is a serial-load register and it can load a new weight value of p bits bit-serially over p cycles. Given that each SWR connects to a different WM wire, they can all concurrently load a different p bit weight value over the same p cycles. Each SIP can then copy its SWR held weight into its WR and proceed with processing the corresponding activations bit-serially. Concurrently with processing the activations, the SWR can proceed to load the next set of weights. Accordingly, loading weights into the SWRs and processing the ones in the WRs form a two “stage” pipeline. The first “stage” of this pipeline requires P_w cycles to load a new set of weights since the weights are loaded bit-serially. The second “stage” of the pipeline requires P_a to process the current set of weights and activations since it multiplies activations bit-serially. As a result, it is the maximum precision of the weights or the activations that will dictate the number of cycles needed to process each group of activations.

Since there are 16 weights per SIP, the SWR and WR are implemented each as a vector of 16 16-bit subregisters. The remainder of this section explains how *TRT* processes CVLs

| Network | Convolutional layers | | Fully-Connected layers | |
|----------------------|--|---------------|---|---------------|
| | Per Layer Activation Precision in Bits | Ideal Speedup | Per Layer Activation and Weight Precision in Bits | Ideal Speedup |
| 100% Accuracy | | | | |
| AlexNet | 9-8-5-5-7 | 2.38 | 10-9-9 | 1.66 |
| VGG_S | 7-8-9-7-9 | 2.04 | 10-9-9 | 1.64 |
| VGG_M | 7-7-7-8-7 | 2.23 | 10-8-8 | 1.64 |
| VGG_19 | 12-12-12-11-12-10-11-11-13-12-13-13-13-13-13 | 1.35 | 10-9-9 | 1.63 |
| NeuralTalk | - | - | 11 (all iterations) | 1.45 |
| Denoise | - | - | 12 (all layers) | 1.33 |
| 99% Accuracy | | | | |
| AlexNet | 9-7-4-5-7 | 2.58 | 9-8-8 | 1.85 |
| VGG_S | 7-8-9-7-9 | 2.04 | 9-9-8 | 1.79 |
| VGG_M | 6-8-7-7-7 | 2.34 | 9-8-8 | 1.80 |
| VGG_19 | 9-9-9-8-12-10-10-12-13-11-12-13-13-13-13 | 1.57 | 10-9-8 | 1.63 |
| NeuralTalk | - | - | 6 (all iterations) | 2.67 |
| Denoise | - | - | 9 (all layers) | 1.77 |

Table 1: Per layer precision profiles needed to maintain the same accuracy as in the baseline. *Ideal*: Potential speedup with bit-serial processing of activations over a 16-bit bit-parallel baseline without dynamic adaptation.

and FCLs. For clarity, in what follows the term *brick* refers to a set of 16 elements of a 3D activation or weight array input which are contiguous along the *channel* dimension, e.g., $a(x, y, i) \dots a(x, y, i + 15)$. Bricks will be denoted by their origin element with a B subscript, e.g., $a_B(x, y, i)$. The size of a brick is a design parameter.

Convolutional Layers: Processing starts by reading in parallel 256 weights from the WM as in *STR*, and loading the 16 per SIP row weights in parallel to all SWRs in the row. Over the next P_a cycles, the weights are multiplied by the bits of an input activation brick per column (P_a is the precision used for activations). *TRT* exploits weight reuse across 16 windows sending a different input activation brick to each column. For example, for a CVL with a stride of 4, a *TRT* tile will process 16 activation bricks $a_B(x, y, i)$, $a_B(x + 4, y, i)$ through $a_B(x + 63, y, i)$ in parallel a bit per cycle. Assuming that the tile processes filters f_i through f_{i+15} , after P_a cycles it would produce 256 *partial* output activations: $o_B(x/4, y/4, f_i), \dots$

$\dots, o_B(x/4 + 15, y/4, f_i)$, that is 16 contiguous on the x dimension output activation bricks. Whereas DPNN would process 16 activations bricks over 16 cycles, *TRT* processes them concurrently but bit-serially over P_a cycles. If P_a is less than 16, *TRT* will outperform DPNN by $16/P_a$, and when P_a is 16, *TRT* will match DPNN’s performance.

Fully-Connected Layers: Processing starts by loading bit-serially and in parallel over P_w cycles 4K weights into the 256 SWRs, 16 per SIP. Each SWR per row gets a different set of 16 weights as each subregister is connected to one out of the 256 wires of the WM output bus for the SIP row (as in DPNN there are $256 \times 16 = 4K$ wires). Once the weights have been loaded, each SIP copies its SWR to its SW and multiplication with the input activations can then proceed bit-serially over P_a^L cycles. Assuming that there are enough output activations so that a different output activation can be assigned to each SIP, the same input activation brick can be broadcast to all SIP columns. For example, for an FCL a *TRT* tile will process one activation brick $a_B(i)$ bit-serially to produce 16 output activation bricks $o_B(i)$ through $o_B(i \times$

16), one per SIP column. Loading the next set of weights can be done in parallel with processing the current set, thus execution time is constrained by $P_{max} = \max(P_a, P_w)$. Thus, a *TRT* tile produces 256 partial output activations every P_{max} cycles, a speedup of $16/P_{max}$ over DPNN since a DPNN tile always needs 16 cycles to do the same.

Cascade Mode: For *TRT* to be fully utilized an FCL must have at least 4K output activations. Some of the networks studied have a layer with as little as 2K output activations. To avoid underutilization, the SIPs along each row are cascaded into a daisy-chain, where the output of one can feed into an input of the next via a multiplexer. This way, the computation of an output activation can be sliced over the SIPs along the same row. In this case, each SIP processes only a portion of the input activations resulting into several partial output activations along the SIPs on the same row. Over the next np cycles, where np the number of slices used, the np partial outputs can be reduced into the final output activation. The user can chose any number of slices up to 16, so that *TRT* can be fully utilized even with fully-connected layers of just 256 outputs. This cascade mode can be useful in some DNNs such as in NeuralTalk [27] where the smallest FCLs can have 600 outputs or fewer.

Other Layers: *TRT* like *STR* can process the additional layers needed by the studied networks. For this purpose the tile includes additional hardware support for max pooling similar to *STR*. An activation function unit is present at the output of output activation buffer in order to apply nonlinear activations before the output neurons are written back to AM.

4.3.1 SIP and Other Components

SIP: Bit-Serial Inner-Product Units: Figure 7 shows *TRT*’s Bit-Serial Inner-Product Unit (SIP). Each SIP multiplies 16 activation bits, one bit per activation, by 16 weights to produce an output activation. Each SIP has two registers, a Serial Weight Register (SWR) and a Weight Register (WR), each containing 16 16-bit subregisters. Each SWR subregister is a shift register with a single bit connection to one of the weight bus wires that is used to read weights bit-serially

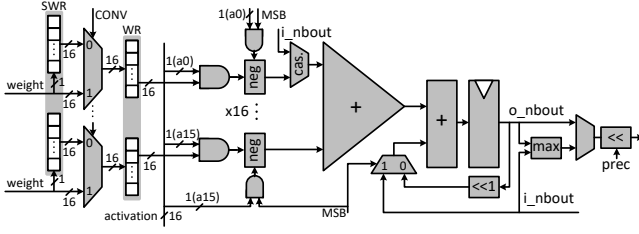


Figure 7: *TRT*'s SIP.

for FCLs. Each WR subregister can be parallel loaded from either the weight bus or the corresponding SWR subregister, to process CVLs or FCLs respectively. Each SIP includes 256 2-input AND gates that multiply the weights in the WR with the incoming activation bits, and a $16 \times 16b$ adder tree that sums the partial products. A final adder plus a shifter accumulate the adder tree results into the output register OR. In each SIP, a multiplexer at the first input of the adder tree implements the cascade mode supporting slicing the output activation computation along the SIPs of a single row. To support signed 2's complement neurons, the SIP can subtract the weight corresponding to the most significant bit (MSB) from the partial sum when the MSB is 1. This is done with negation blocks for each weight before the adder tree. Each SIP also includes a comparator (max) to support max pooling layers. A shifter between the output of the adder tree and the input to the accumulator can be added to support *DPRed*. **Dispatcher and Reducers:** As in *STR* there is a central AM and 16 tiles. A *Dispatcher* unit is tasked with reading input activations from AM always performing eDRAM-friendly wide accesses. It transposes each activation and communicates each a bit a time over the global interconnect. For CVLs the dispatcher has to maintain a pool of multiple activation bricks, each from different window, which may require fetching multiple rows from AM. However, since a new set of windows is only needed every P_a cycles, the dispatcher can keep up for the layers studied. For FCLs one activation brick is sufficient. A *Reducer* per tile is tasked with collecting the output activations and writing them to AM. Since output activations take multiple cycles to produce, there is sufficient bandwidth to sustain all 16 tiles.

4.4 Processing Several Activation Bits at Once

In order to improve *TRT*'s area and power efficiency, the number of activation bits processed at once can be adjusted at design time. The chief advantage of these designs is that less SIPs are needed in order to achieve the same throughput – for example, processing two activation bits at once reduces the number of SIP columns from 16 to 8 and their total number to half. Although the total number of external wires is similar, the distance they have to cover is significantly reduced. Likewise, the total number of adders required stays similar, but they are clustered closer together. A drawback of these configurations is they forgo some of the performance potential as they force the activation precisions to be a multiple of the number of bits that they process per cycle. A designer can choose the configuration that best meets their

area, energy efficiency and performance target.

5. EVALUATION

This section reports *DPRS*'s and *TRT*'s performance, energy, and area comparing to *DPNN* and *STR*. It also explores the trade-off between accuracy and performance for *TRT*. The *TRT* configurations studied here incorporate the *DPRS* technique as well as dynamically adjusting precision for activations.

Section 5.1 describes the experimental methodology. Section 5.2 reports performance, energy efficiency and area measurements for *DPRS*. The section also reports the effect of the number of concurrently processed activations on performance under *DPRS*. Section 5.3.2 evaluates the combination of *DPRS* and *TRT*. For this combination, Section 5.3.4 studies configurations that process two activation bits per cycle.

5.1 Methodology

DPNN, *STR*, *DPRS* and *TRT* were modeled using the same methodology for consistency. A custom cycle-accurate simulator models execution time. Computation was scheduled as described in *STR* to maximize energy efficiency for *DPNN* [18].

Circuit Layouts: To estimate power and area, all tile pipeline designs were synthesized with the Synopsys Design Compiler [28] for a TSMC 65nm library and laid out with Cadence Encounter. Circuit activity was captured with ModelSim and fed into Encounter for power estimation. All designs operate at 980 MHz. The SRAM activation buffers were modeled using CACTI [29]. The AM and WM eDRAM area and energy were modeled with *Destiny* [30]. Three design corner libraries were considered prior to layout as shown in Table 2. The typical case library was chosen for layout as it represents a middle-ground between energy efficiency and area overhead. *DPRS* and *TRT* would improve energy efficiency and performance no matter which design corner was chosen.

Workloads: Given that *DPRS* improves performance only for CVLs, and that *TRT* performs identically to *DPRS* for CVLs while improving performance further only for FCLs, a different set of DNNs is used during the evaluation of the two techniques. For *DPRS* measurements were performed over a set of modern Image Classification CNNs: AlexNet, GoogleNet, NiN, VGG_S, VGG_M, and VGG_19. For these networks CVLs account for than 90% of the execution time. For *TRT* the evaluation omits NiN and GoogleNet since the former has no FCLs and their usage in the latter is not significant. Instead NeuralTalk [27] and Denoise [31] are included that are dominated by FCLs. NeuralTalk uses long short-term memory to automatically generate image captions. Denoise uses 5 FCLs to implement image denoising aiming to reproduce the results of the state-of-the-art BM3D denoising algorithm [32].

5.2 DPRS

5.2.1 Performance

Figure 8 shows the resulting performance improvements with *DPRS* alone and over the equivalently configured

| | Area overhead | Mean efficiency |
|--------------|---------------|-----------------|
| Best case | 39.40% | 0.933 |
| Typical case | 40.40% | 1.012 |
| Worst case | 45.30% | 1.047 |

Table 2: Pre-layout results comparing *TRT* to DPNN with different design libraries. Efficiency values for FCLs.

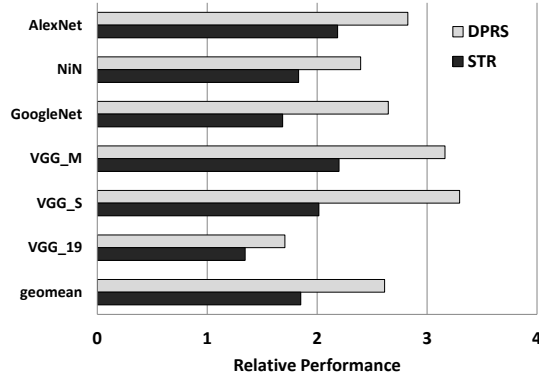


Figure 8: Convolutional Layers: Speedup with DPRS and *STR* over DPNN.

| Network | Effective Precision Per Layer |
|-----------|--|
| AlexNet | 5.39-7.36-4.22-4.40-5.81 |
| NiN | 6.37-7.13-7.79-6.97-5.77-5.15-4.73-6.78 - 8.36-7.51-7.64-7.58 |
| GoogleNet | 6.19-5.94-5.74-6.77-6.91-6.77-6.86-6.77 -6.92-6.31-5.96-6.31-6.00-6.31-6.55-5.33 -5.33-5.33-5.33-5.33-5.48-6.74-6.33-6.74 -6.51-6.74-7.07-6.35-6.17-6.35-5.88-6.35 -6.56-5.07-4.69-5.07-4.82-5.07-5.31-5.53 -4.89-5.53-5.70-5.53-5.86-7.88-7.62-7.88 -8.07-7.88-8.31-4.97-3.85-4.97-3.61-4.97 -5.36 |
| VGG_S | 5.28-5.05-5.82-3.38-4.80 |
| VGG_M | 5.28-5.05-5.04-5.37-4.00 |
| VGG_19 | 9.05-7.69-10.04-9.00-11.08-8.74-9.65-8.29 -11.55-10.37-12.22-11.67-11.53-11.54 -10.40-5.9 |

Table 3: Average Per Layer Activation Precisions with DPRS.

DPNN and *STR*. Since *DPRS* improves performance only for CVLs these measurements are restricted to CVLs only. On average, dynamic prediction reduction boosts performance over *STR* by 41% since *DPRS* proves $2.61\times$ faster than DPNN. Table 3 reports the average precision *DPRS* achieves per layer which when compared to the precisions of Table 5 demonstrates that *DPRS* can effectively reduce precisions.

Figure 9 shows how performance with *DPRS* and relative to DPNN scales for configurations that use different activation group sizes. The range shown is the baseline configuration of 256 activations down to 16 activation groups. Narrower activation groups yield additional benefits and on average *DPRS* with groups of 16 activations is $2.84\times$ faster than an equivalent DPNN configuration.

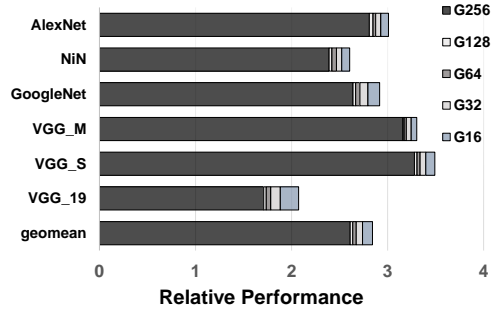


Figure 9: Convolutional Layers: Speedup with DPRS over DPNN for different activation group sizes.

| Network | vs. DPNN | vs. <i>STR</i> |
|-----------|----------|----------------|
| AlexNet | 1.98 | 1.26 |
| NiN | 1.68 | 1.27 |
| GoogleNet | 1.86 | 1.53 |
| VGG_M | 2.22 | 1.40 |
| VGG_S | 2.31 | 1.58 |
| VGG_19 | 1.20 | 1.24 |
| GEOMEAN | 1.84 | 1.38 |

Table 4: Convolutional Layers: Energy Efficiency of DPRS vs. DPNN and vs. *STR*.

5.2.2 Energy Efficiency

As Table 4 shows *DPRS* greatly improves energy efficiency over DPNN and *STR*. The dispatcher has to communicate less bits and the units have to perform fewer calculations. On average, compared to DPNN, *STR* and *DPRS* are $1.84\times$ and $1.38\times$ more energy efficient respectively.

5.2.3 Area

In the interest of space, we omit the detailed area results here and present those for the combination of *DPRS* and *TRT* instead in the respective section. The overall area overhead of dynamic precision reduction is less than 1% over *STR* and as a result *DPRS* is $1.32\times$ larger than DPNN. Given that *DPRS* is $2.61\times$ faster the performance over area ratio is superlinear with *DPRS*. Utilizing 32% more area in DPNN would at best increase performance proportionally. However, in practice the speedup will be a lot less due to filter and input dimensions and filter count.

5.3 DPRS and TRT

5.3.1 Performance

This section evaluates the combination of *DPRS* and *TRT* denoted as *DPRS_T*. Table 5 reports *DPRS_T*'s performance and energy efficiency relative to DPNN for the precision profiles in Table 1 separately for FCLs, CVLs, and the whole network. Denoise has no CVLs. NeuralTalk uses a modified convolutional neural network (based on VGG_16 in this implementation) to recognize objects before the LSTM stage; we have not evaluated that phase as it is similar to the other image classifiers.

On FCLs and for the 100% profile, where no accuracy is

| Accuracy | Fully Connected Layers | | | | Convolutional Layers | | | |
|----------------|------------------------|-------------|-------------|-------------|----------------------|-------------|-------------|-------------|
| | 100% | | 99% | | 100% | | 99% | |
| | Perf | Eff | Perf | Eff | Perf | Eff | Perf | Eff |
| AlexNet | 1.61 | 1.10 | 1.80 | 1.22 | 2.81 | 1.28 | 3.20 | 1.46 |
| VGG_S | 1.61 | 1.09 | 1.76 | 1.19 | 3.26 | 1.49 | 3.49 | 1.59 |
| VGG_M | 1.61 | 1.10 | 1.77 | 1.20 | 3.15 | 1.44 | 3.73 | 1.70 |
| VGG_19 | 1.60 | 1.09 | 1.61 | 1.09 | 1.70 | 0.77 | 2.19 | 1.00 |
| NeuralTalk | 1.42 | 1.01 | 2.60 | 1.85 | - | - | - | - |
| Denoise | 1.30 | 0.92 | 1.53 | 1.09 | - | - | - | - |
| geomean | 1.52 | 1.05 | 1.82 | 1.25 | 2.65 | 1.21 | 3.09 | 1.41 |

Table 5: Execution time and energy efficiency improvement with $DPRS_T$ compared to DPNN.

lost, $DPRS_T$ yields, on average, a speedup of $1.52\times$ over DPNN. With the 99% profile, FCL performance improves to $1.82\times$. For CVLs $DPRS_T$ with the help of $DPRS$ improves performance by $2.65\times$ over DPNN with no accuracy loss. With the 99% accuracy profile, $DPRS_T$ is $3.09\times$ faster than DPNN.

There are two main reasons $DPRS_T$ does not reach the ideal speedup in practice: dispatch overhead and underutilization. Dispatch overhead occurs on the initial P_w cycles of execution, where the serial weight loading process prevents any useful products to be performed. In practice, this overhead is less than 2% for any given network, although it can be as high as 6% for the smallest layers. Underutilization can happen when the number of output activations is not a power of two or lower than 256. The last classifier layers of networks designed to perform recognition of ImageNet categories [33] all provide 1000 output neurons, which results in 2.3% of the SIPs being idle.

5.3.2 Energy Efficiency

This section compares the *Energy Efficiency* or simply *efficiency* of $DPRS_T$ and DPNN. As Table 5 reports, the average efficiency improvement with $DPRS_T$ across all networks and layers for the 100% profile is $1.19\times$. $DPRS_T$ is more efficient than DPNN for both FCLs and CVLs. Overall, efficiency primarily comes from the reduction in effective computation following the use of reduced precision arithmetic for the inner product operations. Furthermore, the amount of data that has to be transmitted from the WM and the traffic between the central eDRAM and the SIPs is decreased proportionally with the chosen precision.

5.3.3 Area

Table 6 reports the area breakdown of $DPRS_T$ and DPNN. Over the full chip, $DPRS_T$ needs $1.51\times$ the area compared to DPNN while delivering on average a $2.59\times$ speedup. Generally, performance would scale sublinearly with area for DPNN due to underutilization. Even under ideal linear scaling DPNN’s performance would have been only $1.51\times$ higher.

5.3.4 Sensitivity to Precision Resolution

This section evaluates the $DPRS_T$ variant of Section 4.4 that processes 2 bits per cycle in as half as many total SIPs. The precisions used are the same as indicated in Table 1 for the 100% accuracy profile rounded up to the next multiple

of two. Table 7 reports the resulting performance. The 2-bit $DPRS_T$ always improves performance compared to DPNN as the “vs. DPNN” columns show. Compared to the 1-bit $DPRS_T$ performance is slightly lower however given that the area of the 2-bit $DPRS_T$ is much lower, this can be a good trade-off. Overall, there are two forces at work that shape performance relative to the 1-bit $DPRS_T$. There is performance potential lost due to rounding all precisions to an even number, and there is performance benefit by requiring less parallelism. The time needed to serially load the first bundle of weights is also reduced. In VGG_M the performance benefit due to the lower parallelism requirement outweighs the performance loss due to precision rounding.

The layout of $DPRS_T$ ’s 2-bit variant requires only 26.0% more area than DPNN (Table 6) while improving energy efficiency in FCLs by $1.24\times$ on average ($1.44\times$ across all layer types).

6. RELATED WORK AND LIMITATIONS

Specialized hardware designs for neural networks is a field with a relatively long history. Bit-serial processing hardware for neural networks has been proposed several decades ago, e.g., [34, 35]. Since then, the size of neural networks has grown and semiconductor technology has progressed, the trade offs (e.g., relative speed of memory vs. transistors vs. wires) involved in these designs are today vastly different.

Distributed Arithmetic (DA), which computes inner products bit-serially, has been used in the design of Digital Signal Processors [36], including designs with application specific dynamic precision detection [37]. The key difference is that DA precomputes all combinations of coefficients and stores them in a lookup table. Applying the same strategy to weights would be intractable due to the large number of weights in modern DNNs.

In general, hardware acceleration for DNNs has recently progressed in two directions: 1) considering more general purpose accelerators that can support additional machine learning algorithms, and 2) considering further improvements primarily for convolutional neural networks and the two most dominant in terms of execution time layer types: convolutional and fully-connected. In the first category there are accelerators such as Cambricon-ACC [38] and Cambricon-X [12]. While targeting support for more machine learning algorithms is desirable, work on further optimizing performance for specific algorithms such as $DPRS$

| | <i>DPRS_T</i> area (mm ²) | <i>DPRS_T</i> 2-bit area (mm ²) | DPNN area (mm ²) |
|---------------------|---|---|------------------------------|
| Inner-Product Units | 58.60 (48.21%) | 38.32 (37.84%) | 17.85 (22.20%) |
| Weight Memory | 48.11 (39.58%) | 48.11 (47.50%) | 48.11 (59.83%) |
| Act. Input Buffer | 3.66 (3.01%) | 3.66 (3.61%) | 3.66 (4.55%) |
| Act. Output Buffer | 3.66 (3.01%) | 3.66 (3.61%) | 3.66 (4.55%) |
| Activation Memory | 7.13 (5.87%) | 7.13 (7.04%) | 7.13 (8.87%) |
| Dispatcher | 0.39 (0.32%) | 0.39 (0.39%) | - |
| Total | 121.55 (100%) | 101.28 (100%) | 80.41 (100%) |
| Normalized Total | 1.51× | 1.26× | 1.00× |

Table 6: Area Breakdown for *DPRS_T* and DPNN.

| | Fully Connected Layers | | Convolutional Layers | |
|------------|------------------------|--------------------------------|----------------------|--------------------------------|
| | vs. BASE | vs. 1b <i>DPRS_T</i> | vs. BASE | vs. 1b <i>DPRS_T</i> |
| AlexNet | +58% | -2.06% | +164% | -7.11% |
| VGG_S | +59% | -1.25% | +191% | -13.27% |
| VGG_M | +63% | +1.12% | +181% | -12.57% |
| VGG_19 | +59% | -0.97% | +63% | -4.93% |
| NeuralTalk | +30% | -9.09% | - | - |
| Denoise | +29% | -1.10% | - | - |
| geomean | +49% | -2.28% | +144% | -9.53% |

Table 7: Relative performance of 2-bit *DPRS_T* variant compared to DPNN and 1-bit *DPRS_T*

and *TRT* is valuable and needs to be pursued as it will affect future iterations of such general purpose accelerators.

Pragmatic uses a similar organization to *STR* and thus *DPRS* but its performance on CVLs depends only on the number of activation bits that are 1 [19]. *DPRed* can be trivially incorporated into the dispatcher unit of *Pragmatic*. This would improve energy efficiency since it would reduce the number of bits sent from AM to the tile. *DPRS* represents a different area, vs. efficiency vs. performance trade off than *Pragmatic*. Finally, it should be possible to apply the *TRT* extension to *Pragmatic*, however, performance in FCLs will still be dictated by weight precision. The area and energy overheads would need to be amortized by a commensurate performance improvement necessitating a dedicated evaluation study.

The *Efficient Inference Engine* (EIE) uses synapse pruning, weight sharing, zero activation elimination, and network retraining to drastically reduce the weight storage and communication when processing fully-connected layers [39]. This is an aggressive form of weight compression requiring a secondary table lookup to decode each weight. *DPRed* attacks activations instead and thus a phenomenon that is mostly orthogonal to those EIE exploits. It may be possible to incorporate *DPRS*'s approach within the tile of EIE. However, this is left for future work. For FCLs, *TRT* offers lightweight memory compression where decoding is simply sign extending the reduced precision weight to the compute precision. An appropriately configured EIE will outperform *TRT* for FCLs, provided that the network is pruned and re-trained.

Cnvlutin is a SIMD accelerator that skips on-the-fly ineffectual activations such as those that are zero or close to zero [11]. SCNN skips both ineffectual activations and weights [10]. SCNN exploits ineffectual weights and activations [10]. Precision variability applies to both effectual

and ineffectual weights and for this reason the phenomenon *DPRed* attacks is mostly different than those SCNN exploits (precision vs. zero-valued activations or weights). Accordingly, investigating whether *DPRed* can be incorporated into SCNN is interesting future work.

Google's Tensor Processing Unit uses quantization to represent values using 8 bits [22] to support TensorFlow [40]. As Table 1 shows, some layers can use lower than 8 bits of precision which suggests that even with quantization it may be possible to use fewer levels and to potentially benefit from *DPRed*.

6.1 Limitations

As in DaDianNao [7] and the TPU [22] this work assumed that each layer fits on-chip. However, as networks evolve it is likely that they will increase in size thus requiring multiple nodes. However, some newer networks tend to use more but smaller layers. Regardless, it would be desirable to reduce the area cost of *TRT* most of which is due to the eDRAM buffers. We have not explored this possibility in this work.

Applying some of the concepts that underlie the *DPRS* and the *TRT* designs to other more general-purpose accelerators such as the Cambricon accelerator family [38] or graphics processors would certainly be more preferable than a dedicated accelerator in most application scenarios. However, these techniques are best first investigated into specific designs and then can be generalized appropriately.

We have evaluated *DPRS* and *TRT* for inference only. Using an engine whose performance scales with precision would provide another degree of freedom for network training as well. However, modifications are needed to support all the operations necessary during training and the training algorithms need to be modified to take advantage of precision adjustments.

This section commented only on related work on digital hardware accelerators for DNNs. Advances at the algorithmic level would impact *DPRS* and *TRT* as well or may even render them obsolete. For example, work on using binary weights [41] would obviate the need for an accelerator whose performance scales with weight precision. However, it is not presently possible to drastically reduce precision for any network at design time.

7. CONCLUSION

We highlighted a previously overlooked property of the runtime calculated value stream of convolutional neural networks. The precision these values need varies considerably and at various granularities. This is a consequence of typical CNN behavior: most values tend to cluster near zero and

only few are further apart. Moreover, the precision needs of these values also greatly depend on the specific input at hand. We thus suggest that hardware accelerator can benefit from this behavior by implementing dynamic prediction reduction.

We demonstrated a practical application that exploits the aforementioned behavior, *DPRed Stripes* an accelerator which trims activation precisions on-the-fly to boost performance and energy efficiency for convolutional layers. Since, fully-connected layers are more important in other workloads, we also proposed *TRT*, a technique to exploit weight precisions in fully-connected layers.

We believe that dynamic prediction reduction opens up several directions for future work including how to combine with other accelerator engines, how it can boost the effectiveness of algorithms for pruning or for precision reduction or quantization of weights and of activations, and whether it can be exploited to accelerate training as well. The accelerators we proposed *do not require* any changes to the input network to deliver benefits. However, they *do reward* any advances in precision reduction including linear quantization and thus if deployed will provide an incentive for further innovation towards networks of extremely low precision.

8. REFERENCES

- [1] A. Delmas, P. Judd, S. Sharify, and A. Moshovos, "Dynamic stripes: Exploiting the dynamic precision requirements of activation values in neural networks," *CoRR*, vol. abs/1706.00504, 2017.
- [2] A. Delmas, S. Sharify, P. Judd, and A. Moshovos, "Tartan: Accelerating fully-connected and convolutional layers in deep learning networks by exploiting numerical precision variability," *CoRR*, vol. abs/1707.09068, 2017.
- [3] Y. LeCun, Y. Bengio, and G. Hinton, "Deep learning," *Nature*, vol. 521, pp. 436–444, 05 2015.
- [4] A. Krizhevsky, I. Sutskever, and G. E. Hinton, "Imagenet classification with deep convolutional neural networks," in *Advances in Neural Information Processing Systems 25: 26th Annual Conference on Neural Information Processing Systems 2012. Proceedings of a meeting held December 3-6, 2012, Lake Tahoe, Nevada, United States.*, pp. 1106–1114, 2012.
- [5] H. Esmailzadeh, E. Blem, R. St. Amant, K. Sankaralingam, and D. Burger, "Dark silicon and the end of multicore scaling," in *Proceedings of the 38th Annual International Symposium on Computer Architecture, ISCA '11*, (New York, NY, USA), pp. 365–376, ACM, 2011.
- [6] T. Chen, Z. Du, N. Sun, J. Wang, C. Wu, Y. Chen, and O. Temam, "Diannao: A small-footprint high-throughput accelerator for ubiquitous machine-learning," in *Proceedings of the 19th international conference on Architectural support for programming languages and operating systems*, 2014.
- [7] Y. Chen, T. Luo, S. Liu, S. Zhang, L. He, J. Wang, L. Li, T. Chen, Z. Xu, N. Sun, and O. Temam, "Dadiannao: A machine-learning supercomputer," in *Microarchitecture (MICRO), 2014 47th Annual IEEE/ACM International Symposium on*, pp. 609–622, Dec 2014.
- [8] Chen, Yu-Hsin and Krishna, Tushar and Emer, Joel and Sze, Vivienne, "Eyeriss: An Energy-Efficient Reconfigurable Accelerator for Deep Convolutional Neural Networks," in *IEEE International Solid-State Circuits Conference, ISSCC 2016, Digest of Technical Papers*, pp. 262–263, 2016.
- [9] S. Han, X. Liu, H. Mao, J. Pu, A. Pedram, M. A. Horowitz, and W. J. Dally, "EIE: Efficient Inference Engine on Compressed Deep Neural Network," *arXiv:1602.01528 [cs]*, Feb. 2016. arXiv: 1602.01528.
- [10] A. Parashar, M. Rhu, A. Mukkara, A. Puglielli, R. Venkatesan, B. Khailany, J. Emer, S. W. Keckler, and W. J. Dally, "Senn: An accelerator for compressed-sparse convolutional neural networks," in *Proceedings of the 44th Annual International Symposium on Computer Architecture, ISCA '17*, (New York, NY, USA), pp. 27–40, ACM, 2017.
- [11] J. Albericio, P. Judd, T. Hetherington, T. Aamodt, N. E. Jerger, and A. Moshovos, "Cnvlutin: Ineffectual-neuron-free deep neural network computing," in *2016 IEEE/ACM International Conference on Computer Architecture (ISCA)*, 2016.
- [12] S. Zhang, Z. Du, L. Zhang, H. Lan, S. Liu, L. Li, Q. Guo, T. Chen, and Y. Chen, "Cambricon-x: An accelerator for sparse neural networks," in *Proceedings of the 49th International Symposium on Microarchitecture*, 2016.
- [13] J. Kim, K. Hwang, and W. Sung, "X1000 real-time phoneme recognition VLSI using feed-forward deep neural networks," in *2014 IEEE International Conference on Acoustics, Speech and Signal Processing (ICASSP)*, pp. 7510–7514, May 2014.
- [14] P. Judd, J. Albericio, T. Hetherington, T. Aamodt, N. E. Jerger, R. Urtasun, and A. Moshovos, "Reduced-Precision Strategies for Bounded Memory in Deep Neural Nets," *arXiv:1511.05236v4 [cs.LG]*, 2015.
- [15] M. Courbariaux, Y. Bengio, and J.-P. David, "BinaryConnect: Training Deep Neural Networks with binary weights during propagations," *ArXiv e-prints*, Nov. 2015.
- [16] P. Warden, "Low-precision matrix multiplication," <https://petewarden.com>, 2016.
- [17] G. Venkatesh, E. Nurvitadhi, and D. Marr, "Accelerating deep convolutional networks using low-precision and sparsity," *CoRR*, vol. abs/1610.00324, 2016.
- [18] P. Judd, J. Albericio, T. Hetherington, T. Aamodt, and A. Moshovos, "Stripes: Bit-serial Deep Neural Network Computing," in *Proceedings of the 49th Annual IEEE/ACM International Symposium on Microarchitecture, MICRO-49*, 2016.
- [19] J. Albericio, A. Delmas, P. Judd, S. Sharify, G. O'Leary, R. Genov, and A. Moshovos, "Bit-pragmatic deep neural network computing," in *Proceedings of the 50th Annual IEEE/ACM International Symposium on Microarchitecture, MICRO-50 '17*, (New York, NY, USA), pp. 382–394, ACM, 2017.
- [20] F. N. Iandola, M. W. Moskewicz, K. Ashraf, S. Han, W. J. Dally, and K. Keutzer, "Squeezenet: Alexnet-level accuracy with 50x fewer parameters and <1mb model size," *CoRR*, vol. abs/1602.07360, 2016.
- [21] B. Moons, R. Uytterhoeven, W. Dehaene, and M. Verhelst, "Envision: A 0.26-to-10tops/w subword-parallel dynamic-voltage-accuracy-frequency-scalable convolutional neural network processor in 28nm fdsoi," in *IEEE Solid-State Circuits Conference (ISSCC)*, 2017.
- [22] N. P. Jouppi, C. Young, N. Patil, D. Patterson, G. Agrawal, R. Bajwa, S. Bates, S. Bhatia, N. Boden, A. Borchers, R. Boyle, P.-I. Cantin, C. Chao, C. Clark, J. Coriell, M. Daley, M. Dau, J. Dean, B. Gelb, T. V. Ghaemmaghami, R. Gottipati, W. Gulland, R. Hagmann, C. R. Ho, D. Hogberg, J. Hu, R. Hundt, D. Hurt, J. Ibarz, A. Jaffey, A. Jaworski, A. Kaplan, H. Khaitan, D. Killebrew, A. Koch, N. Kumar, S. Lacy, J. Laudon, J. Law, D. Le, C. Leary, Z. Liu, K. Lucke, A. Lundin, G. MacKean, A. Maggiore, M. Mahony, K. Miller, R. Nagarajan, R. Narayanaswami, R. Ni, K. Nix, T. Norrie, M. Omernick, N. Penukonda, A. Phelps, J. Ross, M. Ross, A. Salek, E. Samadiani, C. Severn, G. Sizikov, M. Snellman, J. Souter, D. Steinberg, A. Swing, M. Tan, G. Thorson, B. Tian, H. Toma, E. Tuttle, V. Vasudevan, R. Walter, W. Wang, E. Wilcox, and D. H. Yoon, "In-datacenter performance analysis of a tensor processing unit," in *Proceedings of the 44th Annual International Symposium on Computer Architecture, ISCA '17*, (New York, NY, USA), pp. 1–12, ACM, 2017.
- [23] J. Park, S. Li, W. Wen, P. T. P. Tang, H. Li, Y. Chen, and P. Dubey, "Faster CNNs with Direct Sparse Convolutions and Guided Pruning," in *5th International Conference on Learning Representations (ICLR)*, 2017.
- [24] Y. Jia, E. Shelhamer, J. Donahue, S. Karayev, J. Long, R. Girshick, S. Guadarrama, and T. Darrell, "Caffe: Convolutional architecture for fast feature embedding," *arXiv preprint arXiv:1408.5093*, 2014.
- [25] Y. Jia, "Caffe model zoo," <https://github.com/BVLC/caffe/wiki/Model-Zoo>, 2015.
- [26] P. Judd, J. Albericio, T. Hetherington, T. M. Aamodt, N. E. Jerger, and A. Moshovos, "Proteus: Exploiting numerical precision variability in deep neural networks," in *Proceedings of the 2016 International Conference on Supercomputing, ICS '16*, (New York,

NY, USA), pp. 23:1–23:12, ACM, 2016.

- [27] A. Karpathy and F. Li, “Deep visual-semantic alignments for generating image descriptions,” *CoRR*, vol. abs/1412.2306, 2014.
- [28] Synopsys, “Design Compiler.” <http://www.synopsys.com/Tools/Implementation/RTLSynthesis/DesignCompiler/Pages>.
- [29] N. Muralimanoohar and R. Balasubramonian, “Cacti 6.0: A tool to understand large caches.”
- [30] M. Poremba, S. Mittal, D. Li, J. Vetter, and Y. Xie, “Destiny: A tool for modeling emerging 3d nvm and edram caches,” in *Design, Automation Test in Europe Conference Exhibition (DATE), 2015*, pp. 1543–1546, March 2015.
- [31] H. C. Burger, C. J. Schuler, and S. Harmeling, “Image denoising: Can plain neural networks compete with bm3d?,” in *2012 IEEE Conference on Computer Vision and Pattern Recognition*, pp. 2392–2399, June 2012.
- [32] K. Dabov, A. Foi, V. Katkovnik, and K. Egiazarian, “Image denoising with block-matching and 3D filtering,” in *Electronic Imaging 2006*, pp. 606414–606414, International Society for Optics and Photonics, 2006.
- [33] O. Russakovsky, J. Deng, H. Su, J. Krause, S. Satheesh, S. Ma, Z. Huang, A. Karpathy, A. Khosla, M. Bernstein, A. C. Berg, and L. Fei-Fei, “ImageNet Large Scale Visual Recognition Challenge,” *arXiv:1409.0575 [cs]*, Sept. 2014. arXiv: 1409.0575.
- [34] B. Svensson and T. Nordstrom, “Execution of neural network algorithms on an array of bit-serial processors,” in *Pattern Recognition, 1990. Proceedings., 10th International Conference on*, vol. 2, pp. 501–505, IEEE, 1990.
- [35] A. F. Murray, A. V. Smith, and Z. F. Butler, “Bit-serial neural networks,” in *Neural Information Processing Systems*, pp. 573–583, 1988.
- [36] S. White, “Applications of distributed arithmetic to digital signal processing: a tutorial review,” *IEEE ASSP Magazine*, vol. 6, pp. 4–19, July 1989.
- [37] T. Xanthopoulos and A. P. Chandrakasan, “A low-power dct core using adaptive bitwidth and arithmetic activity exploiting signal correlations and quantization,” *IEEE Journal of Solid-State Circuits*, vol. 35, pp. 740–750, May 2000.
- [38] S. Liu, Z. Du, J. Tao, D. Han, T. Luo, Y. Xie, Y. Chen, and T. Chen, “Cambricon: An instruction set architecture for neural networks,” in *2016 IEEE/ACM International Conference on Computer Architecture (ISCA)*, 2016.
- [39] S. Han, X. Liu, H. Mao, J. Pu, A. Pedram, M. A. Horowitz, and W. J. Dally, “EIE: efficient inference engine on compressed deep neural network,” in *43rd ACM/IEEE Annual International Symposium on Computer Architecture, ISCA 2016, Seoul, South Korea, June 18-22, 2016*, pp. 243–254, 2016.
- [40] M. Abadi, A. Agarwal, P. Barham, E. Brevdo, Z. Chen, C. Citro, G. S. Corrado, A. Davis, J. Dean, M. Devin, S. Ghemawat, I. Goodfellow, A. Harp, G. Irving, M. Isard, Y. Jia, R. Jozefowicz, L. Kaiser, M. Kudlur, J. Levenberg, D. Mané, R. Monga, S. Moore, D. Murray, C. Olah, M. Schuster, J. Shlens, B. Steiner, I. Sutskever, K. Talwar, P. Tucker, V. Vanhoucke, V. Vasudevan, F. Viégas, O. Vinyals, P. Warden, M. Wattenberg, M. Wicke, Y. Yu, and X. Zheng, “TensorFlow: Large-scale machine learning on heterogeneous systems,” 2015. Software available from tensorflow.org.
- [41] M. Courbariaux, Y. Bengio, and J.-P. David, “Binaryconnect: Training deep neural networks with binary weights during propagations,” in *Advances in Neural Information Processing Systems*, pp. 3123–3131, 2015.